IEEE Access
Multidisciplinary | Rapid Review | Open Access Journal

Received 13 April 2023, accepted 26 April 2023, date of publication 1 May 2023, date of current version 10 May 2023.

Digital Object Identifier 10.1109/ACCESS.2023.3271716

RESEARCH ARTICLE

Eight Element MIMO Antenna Array With Tri-Band Response for Modern Smartphones

SAAD HASSAN KIANI[1], HUSEYIN SERIF SAVCI[2], (Senior Member, IEEE), HASSAN SANI ABUBAKAR[3], NASER OJAROUDI PARCHIN[4], (Senior Member, IEEE), HATEM RIMLI[1,5], (Senior Member, IEEE), AND BANDAR HAKIM[1]

[1]Electrical and Computer Engineering Department, Faculty of Engineering, King Abdulaziz University, Jeddah 23513, Saudi Arabia
[2]Electrical and Electronics Engineering Department, Faculty of Engineering and Natural Sciences, Istanbul Medipol University, 34810 Istanbul, Turkey
[3]School of Electronics Science and Engineering, University of Electronics Science and Technology of China, Chengdu 610054, China
[4]School of Computing, Engineering and the Built Environment, Edinburgh Napier University, EH10 5DT Edinburgh, U.K.
[5]K. A. CARE Energy Research and Innovation Center, King Abdulaziz University, Jeddah 23513, Saudi Arabia

Corresponding authors: Saad Hassan Kiani (iam.kiani91@gmail.com), Huseyin Serif Savci (hsavci@medipol.edu.tr), and Hatem Rimli (hmrmili@kau.edu.sa)

This work was supported by the Deanship of Scientific Research (DSR) at King Abdulaziz University, Jeddah, under Grant RG-13-135-43.

ABSTRACT This article presents an eight-element tri-band Multiple Input Multiple Output (MIMO) antenna system for future handheld devices. The suggested antenna system consists of a main and sideboards. The feed lines are connected on the main board while the antennas are placed on sideboards, two on each side separately. The total dimension of the main board is 150×75 mm^2, and the sideboard is 150×7 mm^2. The antenna resonates at three distinct 5G allocated bands of 3.1-3.7 GHz, 4.47-4.91 GHz, and 5.5-6.0 GHz with impedance bandwidths of 600 MHz, 440 MHz, and 450 MHz, respectively. The antenna system provides pattern and spatial diversity characteristics with radiation and total efficiency of 78% and 62% and peak gain of 5.8 dBi. The MIMO system is fabricated, and the measured results are found to be in good agreement with the simulations. The isolation among radiating elements in all resonating bands is found to be >16 dB. The vital MIMO performance parameters such as envelope correlation coefficient (ECC) is less than 0.2 for any two antenna array meeting the required standard of less than 0.5 alongside the mean effective gain or MEG ratio of any two antenna meeting the required standard of less than 3 dB for power balance and optimal diversity. The Channel Capacity (CC) is found to be 41.1 bps/Hz, approximately 3 times that of 2×2 MIMO operations.

INDEX TERMS Antenna array, gain, diversity, smartphones, MIMO systems.

I. INTRODUCTION

Electronic communication components can now be tightly packed together to create compact structures with high processing capabilities, such as smartphones and wireless routers, attributable to developing semiconductor technology and sophisticated fabrication techniques [1], [2]. As a result, the multiple antenna configurations effectively utilize the increased computational capacity and increased transmission rate [3], [4], [5]. However, the mobile internet of things (IoT) will become accessible with the availability and improvement of computing mixed with the upgraded radio propagation system or antenna system, which will increase the data rate.The single antenna systems suffer from multipath fading effect. Therefore, to overcome the effects of multipath fading, MIMO technology comes into existence which uses multiple antenna elements in both transmitting and receiving ends without utilizing any additional transmitted power. Furthermore, this technique increases the channel capacity and spatial diversity gain (DG). Recently four-element MIMO operating demonstrations by Ericsson, Telstra, and Qualcomm Technologies are a first step toward commercial network download speeds of 1 Gbps. For a future 5G smartphone, its processing power can be increased to eight and sixteen-element MIMO configurations. Several antenna systems with more than four antenna elements are necessary for such arrangements. The 5G operates in two broad spectrums; the sub6GHz, and the mmWave.

The associate editor coordinating the review of this manuscript and approving it for publication was Ravi Kumar Gangwar.

The mmWave spectrum includes a higher frequency range starting from 24 GHz and above in the Ka-band with potential licensed bands of 26, 28, 32, and 38 GHz [6], [7], [8]. However, at such a high frequency, the propagation loss becomes critical, and the area coverage is only a few kilometers. The mid 5G or sub6GHz band is more practical, with more coverage area and fewer propagation losses. These 5G band includes n46 (5.1-5.9 GHz), n47 (5.5-5.9 GHz), n77 (3.3-4.2 GHz), n78 (3.3-3.7 GHz), n79 (4.4-5 GHz), etc.

In literature, several MIMO systems have been proposed for 5G cellular devices [9], [10], [11], [12], [13], [14], [15], [16], [17], [18], [19], [20]. An eight-element MIMO antenna system presented in [9] resonates from 3.4-3.6.0 GHz frequency. The total size of the antenna is 14 $\times$ 8 mm^2 with isolation >10 dB among resonating elements. A four-element MIMO antenna is reported on a small PCB board of 30 $\times$ 30 mm^2 covering n79 5G band [10]. The antenna offered a peak gain of 2.8 dB with 50% efficiency throughout the resonance bandwidth. In [11], a five-element MIMO antenna system is presented with a decoupling slot. The MIMO antenna comprises four linearly polarized end fire monopoles and one circularly polarized L-shaped radiating element at the center. The reported antenna covered 600 MHz bandwidth for a 5G mid-band of 4.4-5 GHz. The overall size of the antenna was 80 $\times$ 80 mm^2. An eight-element MIMO antenna system is presented in [12] with a resonance band of 4.4-5.0 GHz. The peak isolation is greater than 22 dB with a peak efficiency of 70%. In [13], an eight-element MIMO system is presented with an impedance bandwidth of 3.3-3.6 GHz. The proposed antenna is designed on 150 $\times$ 75 mm^2 PCB, and the minimum isolation reported is >10 dB. In [14], a hybrid eight-element antenna was presented, resonating at two distinct 5G bands of 2.6 and 3.5GHz. The arrangement of the MIMO antennas was such that the side antennas were mounted on the main board while the mid-radiating elements were placed on side substrates. In literature, Dual-band MIMO antenna systems are also reported, which minimizes the need to accommodate more radiating elements on boards. In [15], a dual-band antenna system is presented with the resonance of 3.4-3.6 GHz and 5.1-5.9 GHz with an efficiency ranging from 60-70%. A dual band antenna system in [16] showed resonance on 3.5 and 5.8 GHz systems with bandwidth exhibiting 200 MHz and 900 MHz with peak efficiency of 70% and ECC less than 0.2. Similarly, in [17], a planar inverted L shape MIMO antenna with a ground slot is presented with the dual resonance of 3.5 and 5.6 GHz having minimum isolation of >13dB. An eight-element MIMO antenna for the sub-6 GHz and LTE band 42 was presented in [18]. The antenna elements were printed on the side-edge frame of the smartphone. A decoupling structure was designed between the antenna elements to achieve high isolation. The designed MIMO antenna offers an impedance bandwidth of 300 MHz from 3.3 to 3.6 GHz. Furthermore, the addition of the decoupling structure excited a new resonance in the frequency range of 2.4×2.7 GHz. In [19] an eight element MIMO System is presented covering n79 band from 4.6-5.0 GHz with isolation <18dB. Moreover in [20] a dual-band MIMO system is reported covering 3.4-3.6 and 4.8-5.0 GHz resonance bandwidth with isolation <15dB among radiating elements.

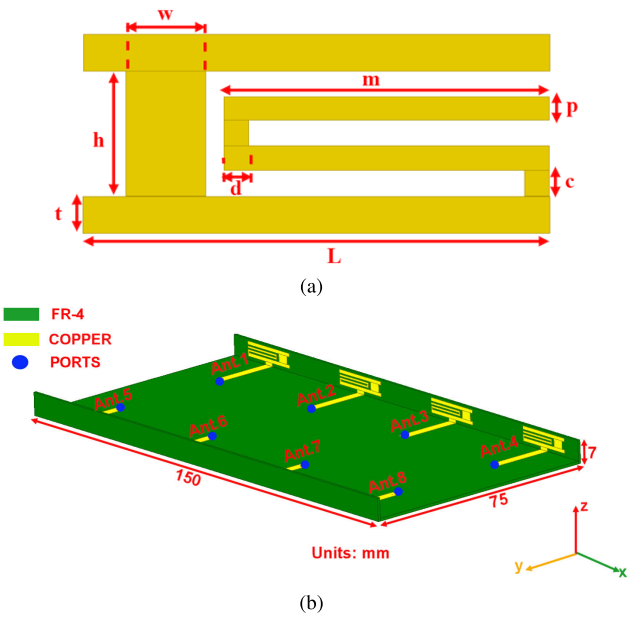

FIGURE 1. Proposed MIMO antenna system (a) Single element (b) Overall view.

Multiple antenna structures for MIMO applications, as mentioned, vary in size and geometry and typically cover a certain frequency band. In this study, we propose a single antenna design that covers multiple bands of 5G NR operation. Although it has three resonances, several bands can be served with partial or full coverage. The antenna's first band is functional for n77, n78, and n47 operations of 5G, the second resonance is good for n79, and the third resonance is operational on n46 and n47. The 5G NR radios operating at the sub-6GHz region have many allocated bands. A cost-effective system solution would be an antenna covering as many bands as possible. The 5G handsets generate interference to other wireless links and are susceptible to unwanted signals from other bands when an ultra-wideband antenna solution is adopted. This work proposes an antenna that is only functional in 5G NR bands and rejects others with less complexity, helpful to employ intra-band contiguous carrier aggregation to increase the data throughput and applicable to a future 5G smartphone.

II. ANTENNA DESIGN

The detailed procedure to design eight slot antenna structure for the implementation of MIMO operation in a smartphone is discussed in this section. The proposed MIMO antenna is designed on a commercially available low-cost 0.8 mm thin FR4 substrate with relative permittivity of 4.4. The board size is kept 150 $\times$ 75 mm^2 per modern smartphone size, and the side substrate is kept 7 $\times$ 150 mm^2.

TABLE 1. MIMO antenna dimension.

Parameter	Value in mm	Parameter	Value in mm
L_{SUB}	150	W_{SUB}	75
L	18	t	1
c	0.5	d	0.5
h	3.5	w	2.5
m	12.5	p	0.5

Fig. 1 shows the proposed MIMO antenna system. The arrangement of antennas is made in such a way that every side has four antenna elements, each connected with a feed line. The length of the feed line is 19 × 3 mm^2. Table. 1 shows the detailed dimensions of the MIMO system.The proposed MIMO system consists of common ground plane of 150 × 75 mm. In general, MIMO antenna systems should have a common ground plane rather than separated ground plane, for proper interpretation of signal levels based on the reference level. Although separated ground plane provides good isolation, in a real system it is not practical.

Fig. 2 shows the design evolution of the proposed antenna. The reflection coefficient response during evolving stages is shown in Fig. 3. The effective length of the radiating element at each stage has been derived using the following equation. It is shown that the total length of corresponding segments in each stage contributes to the related resonance frequency by comparing it with the effective length of the resonance.

$$L_{eff} = \frac{C}{2f_0\sqrt{\epsilon_{reff}}} \tag{1}$$

where C is the speed of light, f_0 is the operating frequency and ϵ_{reff} is the effective dielectric constant

$$\epsilon_{reff} = \frac{\epsilon_r + 1}{2} \tag{2}$$

which is calculated as 2.6 for the FR-4 substrate.

At the start, the lower bottom part of the radiating element is constructed as Stage 1. It is a T shape structure with a vertical feedline and horizontal resonating element. The T shape structure, generated resonance at a higher band of 5.48 GHz, as seen in Fig. 3. When the feedline width is subtracted, the total length of this segment would be equal to L − t = 17mm, which is equal to Leff=17 mm. This is the effective half-wavelength of 5.48 GHz resonance. So this segment generated resonance at 5.48 GHz. In the next step, an inverted L shape strip is introduced, as highlighted in red. The combination of the segments of the new radiating stub and the partial segment of the T structure generates low-band resonance. This is in addition to the high-band resonance making the entire Stage 2 a dual-band resonator. Low-band resonance comes from the addition of the length of the T-structure half segment when the feedline width is subtracted, and the total length of vertical and horizontal segments when the width is subtracted. So the total is (L − t)/2 + h + L − w = 27.5 mm, which is the effective half-wavelength of the 3.38 GHz resonance. So the addition of an inverted L shape strip enabled the generation of low-band resonance. Lastly, the right side of the antenna is introduced with one C shape strip connected from the bottom-right end to the top-right end of the T shape radiating element. The longer segments of this structure are parallel and very close to each other. The opposite-direction flowing currents cause the cancellation of fields due to the very close proximity. Therefore their effective contribution to the resonance is much less than their physical length. The new addition of Stage 3 is designed to generate the mid-band resonance in such a small area. The total length of the segments can be calculated by considering the reduced length effective contribution of m segments and the T-structure half segment when the widths of T-lines are subtracted. The total length can be calculated as (L − t)/2 − d + c − d + m − d + c − d + m = 20 mm. The effective half-wavelength of the 4.65 GHz resonance is also 20 mm. So we can conclude that the addition of the C structure resulted in generating the mid-band resonance of 4.65 GHz in addition to the other two bands.

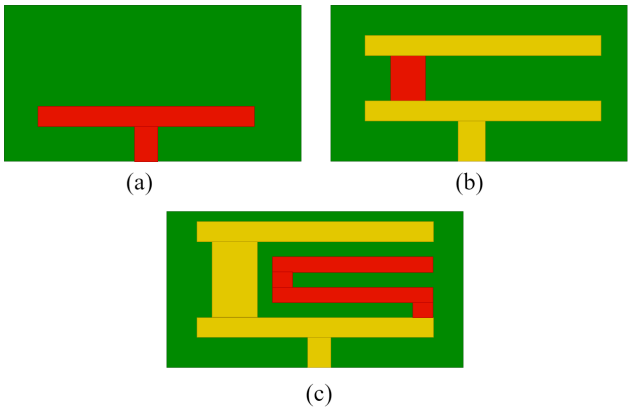

FIGURE 2. Proposed design evolution (a) Stage 1 (b) Stage 2 (c) Stage 3 (proposed).

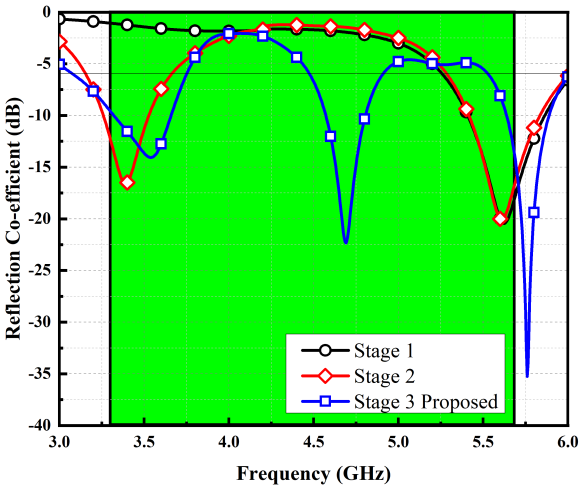

FIGURE 3. Design evolution S-parameters.

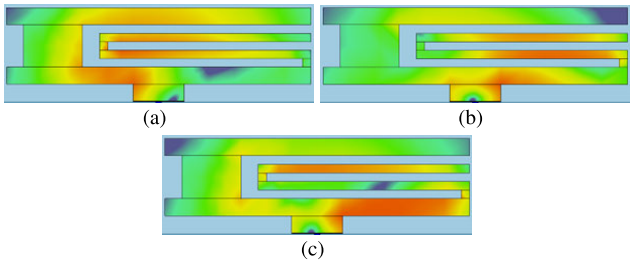

FIGURE 4. Surface current distribution (a) 3.5GHz (b) 4.7GHz (c) 5.75GHz.

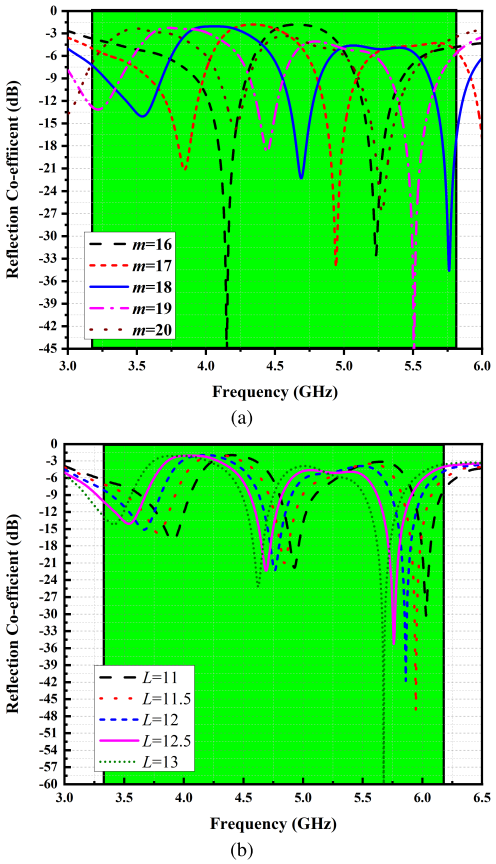

FIGURE 5. Parametric analysis of strip (a) m (b) L.

This effect can be observed by looking at Fig.4, which shows the surface current distribution for a single antenna element. From the figure, it can be observed that at the first resonance, the current is concentrated at the higher region of the antenna element i-e, T and L shape strips, while for the second resonance, the current is more focused at C shape strips. This shows that the mid-resonance can be attributed to the C shape resonator in the proposed antenna. The last resonance, at 5.7 GHz, can be attributed to the T shape and upper strip of the C shape resonator, which shows that both elements are partially responsible for generating the response.

III. PARAMETRIC ANALYSIS

Fig. 5 presents the parametrical analysis on resonating strips and stubs to observe a single-element antenna's resonance response. For this purpose, the physical parameters m and L strips were analyzed. As seen in Fig. 5, the resonance frequency at m=18 mm shows the desired response. This response moves forward to the lowest resonance of 4.1 GHz with a second resonance at 5.2 GHz when the length of the L strip is 16 mm. Similarly, as the length of the strip is increased further, the resonance response moves to lower levels. This effect in shifting resonance can be seen since the physical dimensions of the antenna, when changed, increases the path of the current induced in it. As the structure's length increases, the resonance frequency is shifted forward. Compared to parameter m, the L parameter was observed to be less sensitive to resonance response. As the strip length increased, the resonance response moved forward. Also, the first and third resonance impedance was found to be varied, and opposite. At 11 mm, the first resonance was found nearly 4 GHz and the third at 6 GHz. At 13 mm, the first resonance response started to diminish. The optimum value was found to be 12 mm. The optimized MIMO S-parameters response is shown in Fig. 5.

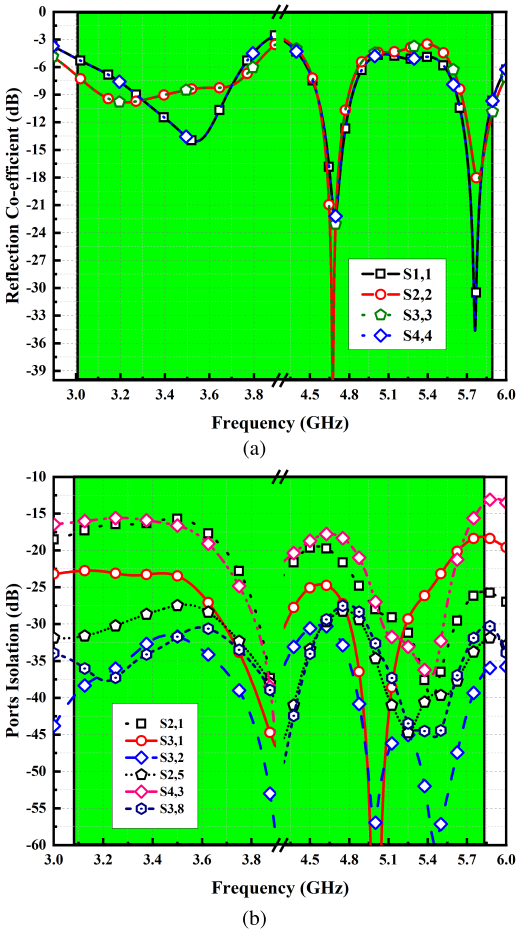

FIGURE 6. S-parameters simulated (a) reflection co-efficient and (b) coupling.

The isolation among all radiating elements is >16 dB throughout the bandwidth. For the sake of simplicity, only one side of the MIMO system is presented.

The peak gain achieved is 5.5 dBi at 5.8 GHz, while for 3.5 and 4.7 GHz, it's noted to be 4.5 and 5.2 dBi. The radiation and total efficiency of Ant1 and Ant2 with gain are shown in Fig. 7 and Fig. 8. It can be seen that the total efficiency of the antenna is $> 60\%$ for all resonance bands while the peak efficiency is noted at 80% at the first resonance of 3.5 GHz while the total efficiency ranges in between 50-70%.

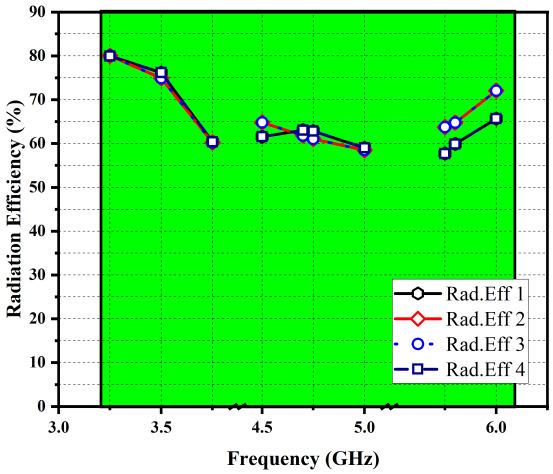

FIGURE 7. Radiation efficiency of MIMO antenna.

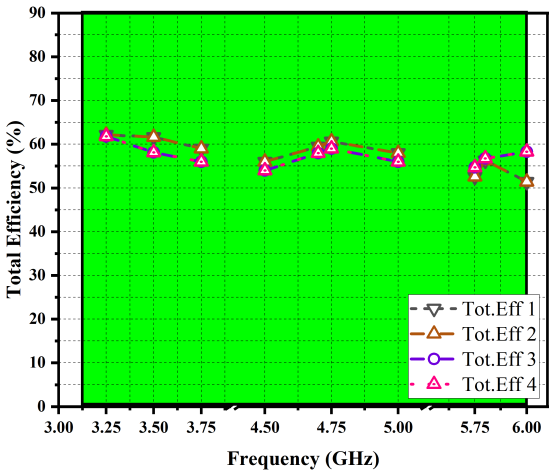

FIGURE 8. Total efficiency of MIMO antenna.

IV. RESULT AND DISCUSSIONS

The proposed eight-element MIMO antenna system is fabricated and tested using the in-house facility. The fabricated prototype before and after assembly is shown in Fig. 9. The measured results obtained are mentioned in Fig 10. Fig. 9(a) shows the prototype of the proposed antenna model before assembling, while Fig 9(b) shows the back side of the antenna with connectors after assembling. Fig. 9(c) shows the front side of the fabricated prototype after assembling.

A. S-PARAMETERS

From the figure, one can also observe from the result of Fig. 10, that the antenna elements provide different

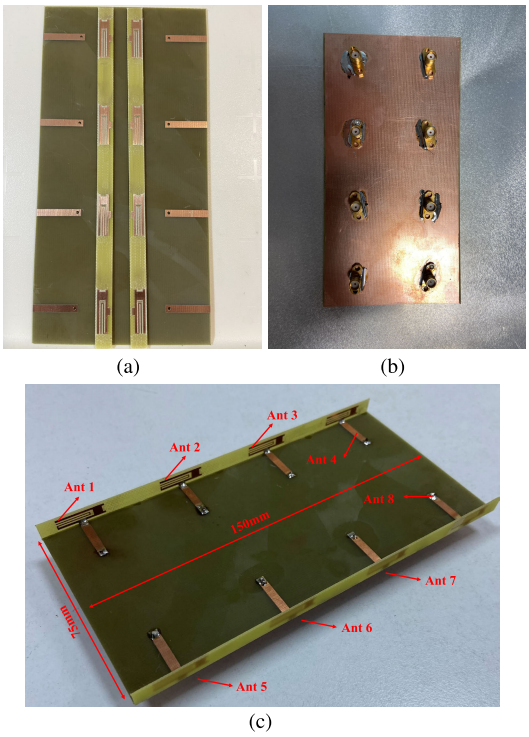

FIGURE 9. Fabricated prototype (a) Front without assembling (b) Back with assembling. (c) Front with assembling.

bandwidths for all frequency bands. Furthermore, it has been observed from Fig. 10(b) that the measured isolation between the antenna elements is much better compared to the simulated one. A discrepancy between the simulated and measured results could arise due to fabrication tolerances, coaxial connector losses, etc.

B. RADIATION PATTERNS

The far-field radiation characteristics of the presented MIMO antenna are assessed using a traditional spherical near-field anechoic chamber. A dual-ridge horn antenna with a flat gain response across the 1-18 GHz frequency range is employed as a reference antenna. The designed MIMO antenna is mounted from the back using double-sided tapes to the wooden rod of the turntable on the opposite side.

Due to the mirror symmetry of the array structure, the elements should have the same radiation characteristics in symmetrical positions in theory but in opposite planes. For simplification, only one side of the elements is being studied, which includes Ant1, Ant2, Ant3, and Ant4. The simulated and measured radiation patterns in the *yz* and *yx* planes are shown in Fig.11, 12, and 13. It is clear that the radiation patterns of Ant1 and Ant4 at 3.5 GHz on the *yz* plane are observed to be at 315°, while on the *yx* plane, they are at 225° and 135° respectively. Similarly, the radiation patterns of Ant2 and Ant3 at 3.5 GHz and 4.7 GHz are similar in both planes with maximum radiation at 310° and 90° along the *yz* and *yx* planes. Fig. 13 shows the plot of Ant1 and Ant4

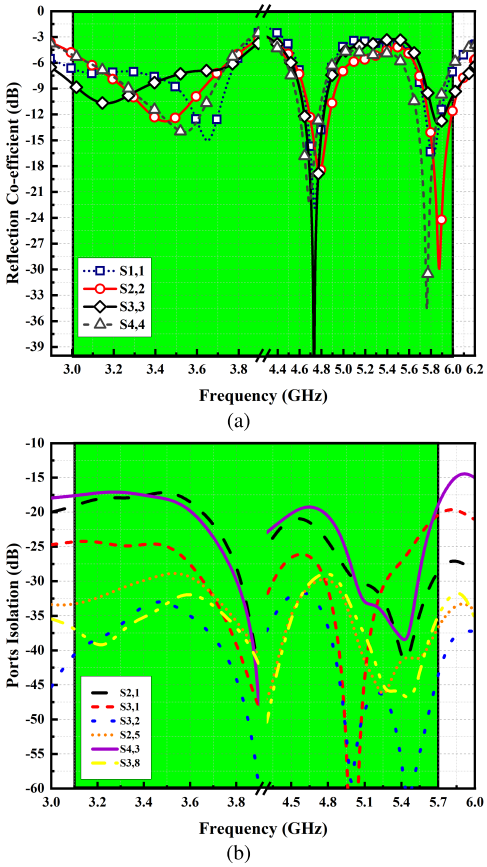

FIGURE 10. Measured S-parameters (a) Reflection co-efficient and (b) Ports isolation.

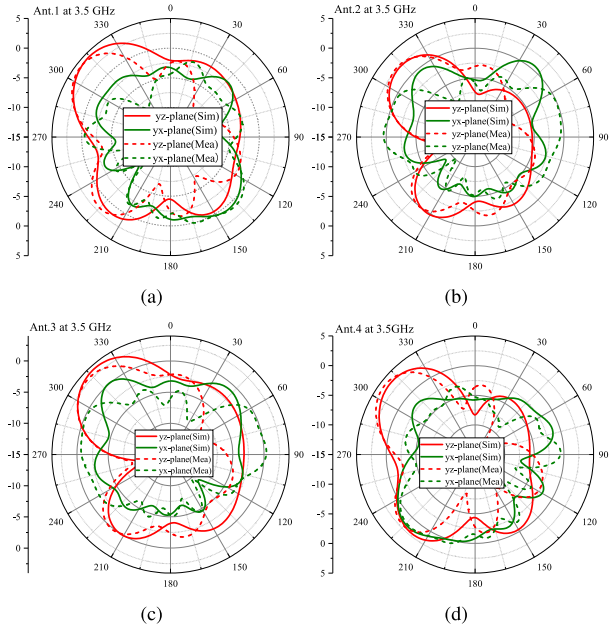

FIGURE 11. Simulated and measured radiation plots at 3.5GHz (a) Ant1 (b) Ant2 (c)Ant3 (d)Ant4.

at 4.7GHz. The antennas display a strong radiation pattern at 300° and 120° on the *yz* plane, while on the *yx*-plane, the radiation is at 150° for Ant1 and 210° for Ant4.

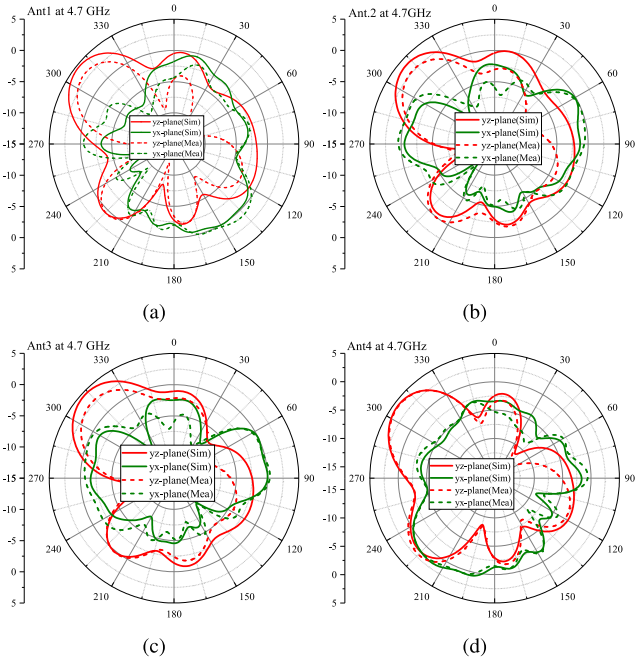

FIGURE 12. Simulated and measured radiation plots at 4.7GHz (a) Ant1 (b) Ant2 (c)Ant3 (d)Ant4.

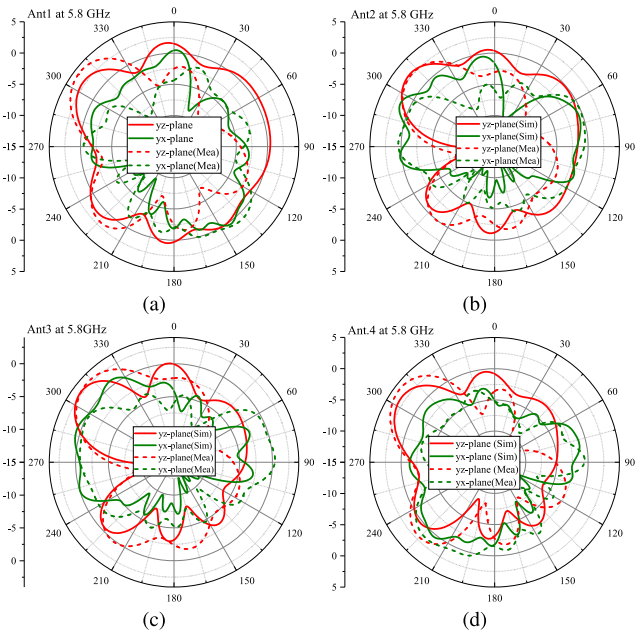

FIGURE 13. Simulated and measured radiation plots at 5.8GHz (a) Ant1 (b) Ant2 (c)Ant3 (d)Ant4.

Almost a quasi-omnidirectional radiation pattern is seen for Ant1 at 5.8 GHz on the *yz*-plane with strong radiation towards 130° for the same antenna on the *yx*-plane. The pattern for Ant.4 at 5.8 GHz remains the same as when the antenna radiate at 3.5 GHz. From Fig.13, a butterfly-like shape pattern for Ant.2 and 3 at 5.8 GHz along the *yz*-axis is observed, with ±190° radiation on the yx-plane. Although slight variations exist between the measured and simulated

results, the two findings have a general similarity. The small discrepancy is attributed to the test settings. To sum up, the diversity of maximum radiation orientations leads to a diverse pattern, improving the MIMO antenna's overall performance.

V. MIMO PARAMETERS

In order to verify the MIMO parameters characteristics, the proposed MIMO system parameters, such as Envelope co-relation co-efficient (ECC), Diversity Gain (DG), and ergodic channel capacity (CC), are calculated.

A. ENVELOPE CORRELATION COEFFICIENT

ECC shows how well antennas in MIMO systems are isolated. The ECC is derived from far-field parameters using the equation below [21], [22]. For practical applications, the ECC values should be less than 0.5. Fig. 14 shows the simulated and measured value of ECC for the proposed MIMO system.

$$ECC = \frac{|\iint_{4\pi}(\vec{B}_i(\theta,\phi)) \times (\vec{B}_j(\theta,\phi))\, d\Omega|^2}{\iint_{4\pi}|(\vec{B}_i(\theta,\phi))|^2\, d\Omega \iint_{4\pi}|(\vec{B}_j(\theta,\phi))|^2\, d\Omega} \quad (3)$$

where $\vec{B}_i(\theta,\phi)$ denotes the 3D radiation pattern upon excitation of the i^{th} antenna and $\vec{B}_j(\theta,\phi)$ denotes the 3D radiation pattern upon excitation of the j^{th} antenna. Ω is the solid angle.

From the figure, it can be seen that the ECC value is less than 0.035 for the entire operating bandwidth. The ECC for the antenna elements facing each other such as Ant 5 and Ant 2, is 0.035. As for Ant 1 and Ant 2, ECC is found to be 0.025 and below.

B. DIVERSITY GAIN

Another important feature that needs to be assessed is DG. The DG of the MIMO antennas should be high ≈10 dB in the operating bandwidth [23], [24]. It is expressed in terms of ECC as:

$$DG = 10\sqrt{1 - (ECC^2)} \quad (4)$$

The diversity gain and correlation coefficient are related to each other; the lower the correlation coefficient, the higher the diversity gain. As seen in Fig. 15, the diversity gain value is higher than 9.84.

C. CHANNEL CAPACITY

This section presents the proposed MIMO system's calculated ergodic channel capacity (cc). The cc is calculated by averaging 10,000 realizations of Rayleigh fading with a reference signal-to-noise ratio (SNR) of 20 dB. Rayleigh fading model provides a useful framework for modeling wireless communication channels that experience random fluctuations due to multi-path propagation. Fig. 16 shows the proposed cc of the proposed MIMO system. The figure shows that the cc ranges from 38 to 41bps/Hz, close to the ideal range. The CC is calculated using the following equation.

$$C = B * \log_2(1 + SNR) \quad (5)$$

where C is the Channel capacity in bps, and B is the allocated bandwidth.

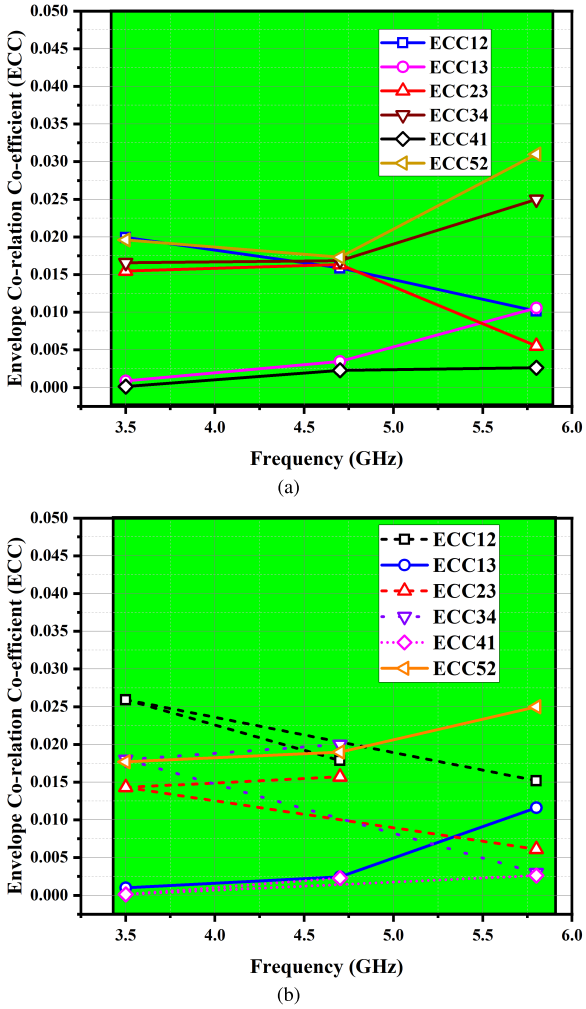

FIGURE 14. ECC of the proposed MIMO system (a) Simulated and (b) measured.

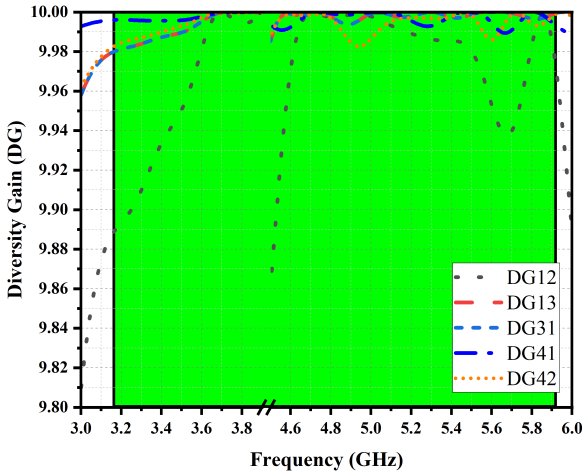

FIGURE 15. Diversity gain of MIMO antenna.

D. TOTAL ACTIVE REFLECTION CO-EFFICIENT

In MIMO antenna systems, the Total Active Reflection Coefficient (TARC) is an important parameter that quantifies the

TABLE 2. Comparison with other published work.

Ref	Frequency	Board size	Antenna Size	Port Isolation	Efficiency(%)	ECC	CC
[10]	3.4-3.6	150×75	14×8	<10	45-60	0.3	39.1
[11]	4.7-5.1	40×40	5.1×18	<25	67-72	0.01	17
[12]	4.5-5.0	80×80	6×12	<15	N/A	0.02	N/A
[13]	3.4-3.6	150×75	12.5×18.5	<12	42-65	0.2	38
[14]	2.6-3.6	150×75	15×3	<13	45-65	0.2	34.25
[15]	3.4-3.6/5.1-5.9	150×75	14.9×4	<12	60-65/58-70	0.2	40
[16]	3.4-3.6/5.4-5.8	150×75	2.5×11.5	<15	63-69/54-78	0.15	39.5
[17]	3.4-3.8/5.1-5.9	150×80	6.3×4.3	<11	42-65/62-68	0.15	N/A
[18]	2.4-2.7/3.4-3.6	150×75	6.8×6	<14	40-58/60-70	0.2	N/A
[19]	4.4-5.0	150×75	5.77×7.8	<18.5	50-65/65-75	0.1	40.2
[20]	3.4-3.6/4.8-5.0	150×75	15×7	<11.5	40-65/78-42	0.08	38.5
Prop.	3.1-3.7/4.47-4.9/5.6-6.0	150×75	4.5×18	<16	78-55	0.02	41.1

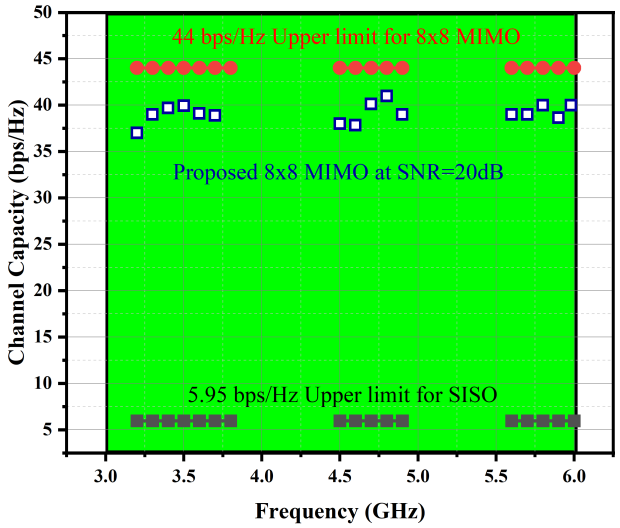

FIGURE 16. Channel capacity of MIMO antenna.

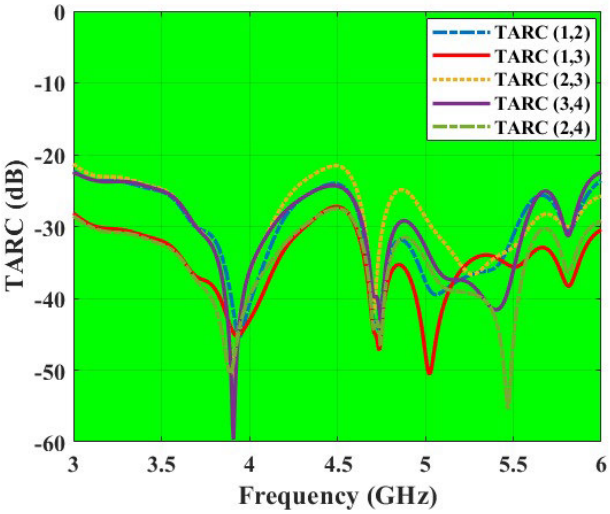

FIGURE 17. TARC of proposed MIMO antenna.

performance of the antenna system in terms of its ability to transmit and receive signals with minimal reflection losses. A low TARC value in a MIMO antenna system implies that the system effectively transmits and receives signals with minimal losses due to reflection. This results in improved signal quality, higher data rates, and increased system capacity. The TARC of the proposed MIMO system is shown in Fig. 17 by the method described in [21] and [22], which shows that the values are well below the −10 dB level within the desired bands.

A comparison among proposed and previously presented MIMO antennas are presented in Table 2. The data in the table shows that the proposed MIMO antenna offers good performance characteristics with low ECC and higher CC values.

VI. CONCLUSION

This work presents a novel shape eight-element MIMO antenna system. The proposed antenna resonated at three different bands dedicated to 5G communication. The antenna's bandwidth included 3.1-3.7 GHz, 4.47-4.91 GHz, and 5.5-6.0 GHz with peak radiation and total efficiency of 78% and 62%. The ECC among any two radiating elements is less than 0.03, and the calculated peak channel capacity is 41.1 bps/Hz, approximately 3 times that of 2 × 2 MIMO operations. The measured results obtained from the fabricated prototype agree well with the simulations. Through performance characteristics and results obtained, the proposed MIMO system can be termed as a potential candidate for future cellular devices.

ACKNOWLEDGMENT

The authors acknowledge the support provided by King Abdullah City for Atomic and Renewable Energy (K. A. CARE) under K. A. CARE-King Abdulaziz University Collaboration Program.

REFERENCES

[1] M. Farasat, D. N. Thalakotuna, Z. Hu, and Y. Yang, "A review on 5G sub-6 GHz base station antenna design challenges," *Electronics*, vol. 10, no. 16, p. 2000, Aug. 2021.

[2] A. Goudarzi, M. M. Honari, and R. Mirzavand, "Resonant cavity antennas for 5G communication systems: A review," *Electronics*, vol. 9, no. 7, p. 1080, Jul. 2020.

[3] S. H. Kiani, A. Iqbal, S.-W. Wong, H. S. Savci, M. Alibakhshikenari, and M. Dalarsson, "Multiple elements MIMO antenna system with broadband operation for 5th generation smart phones," *IEEE Access*, vol. 10, pp. 38446–38457, 2022.

[4] N. O. Parchin, H. J. Basherlou, Y. I. A. Al-Yasir, A. Ullah, R. A. Abd-Alhameed, and J. M. Noras, "Multi-band MIMO antenna design with user-impact investigation for 4G and 5G mobile terminals," *Sensors*, vol. 19, no. 3, p. 456, Jan. 2019.

[5] G. Kim and S. Kim, "Design and analysis of dual polarized broadband microstrip patch antenna for 5G mmWave antenna module on FR4 substrate," *IEEE Access*, vol. 9, pp. 64306–64316, 2021.

[6] I.-J. Hwang, J.-I. Oh, H.-W. Jo, K.-S. Kim, J.-W. Yu, and D.-J. Lee, "28 GHz and 38 GHz dual-band vertically stacked dipole antennas on flexible liquid crystal polymer substrates for millimeter-wave 5G cellular handsets," *IEEE Trans. Antennas Propag.*, vol. 70, no. 5, pp. 3223–3236, May 2022.

[7] S. H. Kiani, A. G. Alharbi, S. Khan, M. Marey, H. Mostafa, and M. A. Khan, "Wideband three loop element antenna array for future 5G mmWave devices," *IEEE Access*, vol. 10, pp. 22472–22479, 2022.

[8] M. A. Khan, A. G. Al Harbi, S. H. Kiani, A. N. Nordin, M. E. Munir, S. I. Saeed, J. Iqbal, E. M. Ali, M. Alibakhshikenari, and M. Dalarsson, "mmWave four-element MIMO antenna for future 5G systems," *Appl. Sci.*, vol. 12, no. 9, p. 4280, Apr. 2022.

[9] M. N. Hossain, L. C. Paul, M. A. Rahim, and J. Shin, "Multiband slotted crescent-shaped patch antenna for K-band satellite and mmWave communications," *IEIE Trans. Smart Process. Comput.*, vol. 11, no. 3, pp. 213–221, Jun. 2022.

[10] S. H. Kiani, A. Altaf, M. Abdullah, F. Muhammad, N. Shoaib, M. R. Anjum, R. Damaševičius, and T. Blažauskas, "Eight element side edged framed MIMO antenna array for future 5G smart phones," *Micromachines*, vol. 11, no. 11, p. 956, Oct. 2020.

[11] H. Ali, X.-C. Ren, I. Bari, M. A. Bashir, A. M. Hashmi, M. A. Khan, S. I. Majid, N. Jan, W. U. K. Tareen, and M. R. Anjum, "Four-port MIMO antenna system for 5G n79 band RF devices," *Electronics*, vol. 11, no. 1, p. 35, Dec. 2021.

[12] R. K. Jaiswal, K. Kumari, A. K. Ojha, and K. V. Srivastava, "Five-port MIMO antenna for n79-5G band with improved isolation by diversity and decoupling techniques," *J. Electromagn. Waves Appl.*, vol. 36, no. 4, pp. 542–556, Mar. 2022.

[13] S. H. Kiani, A. Altaf, M. R. Anjum, S. Afridi, Z. A. Arain, S. Anwar, S. Khan, M. Alibakhshikenari, A. Lalbakhsh, M. A. Khan, R. A. Abd-Alhameed, and E. Limiti, "MIMO antenna system for modern 5G handheld devices with healthcare and high rate delivery," *Sensors*, vol. 21, no. 21, p. 7415, Nov. 2021.

[14] M. Abdullah, S. H. Kiani, and A. Iqbal, "Eight element multiple-input multiple-output (MIMO) antenna for 5G mobile applications," *IEEE Access*, vol. 7, pp. 134488–134495, 2019.

[15] H. Zou, Y. Li, C.-Y.-D. Sim, and G. Yang, "Design of 8 × 8 dual-band MIMO antenna array for 5G smartphone applications," *Int. J. RF Microw. Comput.-Aided Eng.*, vol. 28, p. 112, Jun. 2018.

[16] H. Ali, X.-C. Ren, A. M. Hashmi, M. R. Anjum, I. Bari, S. I. Majid, N. Jan, W. U. K. Tareen, A. Iqbal, and M. A. Khan, "An eight element dual band antenna for future 5G smartphones," *Electronics*, vol. 10, no. 23, p. 3022, Dec. 2021.

[17] J. Li, X. Zhang, Z. Wang, X. Chen, J. Chen, Y. Li, and A. Zhang, "Dual-band eight-antenna array design for MIMO applications in 5G mobile terminals," *IEEE Access*, vol. 7, pp. 71636–71644, 2019.

[18] W. Jiang, Y. Cui, B. Liu, W. Hu, and Y. Xi, "A dual-band MIMO antenna with enhanced isolation for 5G smartphone applications," *IEEE Access*, vol. 7, pp. 112554–112563, 2019.

[19] Y. Gao, J. Wang, X. Wang, and R. Shao, "Miniaturized MIMO antenna array with high isolation for 5G metal-frame smartphone application," *Micromachines*, vol. 13, no. 7, p. 1064, Jul. 2022.

[20] J. Guo, L. Cui, C. Li, and B. Sun, "Side-edge frame printed eight-port dual-band antenna array for 5G smartphone applications," *IEEE Trans. Antennas Propag.*, vol. 66, no. 12, pp. 7412–7417, Dec. 2018.

[21] S. Modak, S. Daasari, P. P. Shome, and T. Khan, "Switchable/tunable band-notched characteristics in UWB and UWB-MIMO antennas: A comprehensive review," *Wireless Pers. Commun.*, vol. 128, pp. 1–24, Sep. 2022, doi: 10.1007/s11277-022-10036-1.

[22] K. Srivastava, B. K. Kanaujia, S. Dwari, S. Kumar, and T. Khan, "3D cuboidal design MIMO/diversity antenna with band notched characteristics," *AEU-Int. J. Electron. Commun.*, vol. 108, pp. 141–147, Aug. 2019, doi: 10.1016/j.aeue.2019.06.018.

[23] S. Modak and T. Khan, "A slotted UWB-MIMO antenna with quadruple band-notch characteristics using mushroom EBG structure," *AEU-Int. J. Electron. Commun.*, vol. 134, May 2021, Art. no. 153673.

[24] S. Modak and T. Khan, "Cuboidal quad-port UWB-MIMO antenna with WLAN rejection using spiral EBG structures," *Int. J. Microw. Wireless Technol.*, vol. 14, no. 5, pp. 626–633, Jun. 2022.

SAAD HASSAN KIANI received the B.S. degree from the City University of Science and Information Technology, in 2014, the M.S. degree from Iqra National University, in 2018, and the Ph.D. degree from the IIC University of Technology, Cambodia, in 2022. He was a part of the Smart Systems Engineering Laboratory, College of Engineering, Prince Sultan University, Saudi Arabia, from July 2022 to January 2023. He is currently a Research Scientist with the RFMicroSense Research Group, Istanbul Medipol University, Istanbul, Turkey; and the Advance Electromagnetics Research Group, King Abdulaziz University, Jeddah, Saudi Arabia. His research interests include MIMO antenna systems, slot antennas, origami and kirigami antennas, multiband antennas, and metasurfaces.

HUSEYIN SERIF SAVCI (Senior Member, IEEE) received the B.S. degree in electronics and communication engineering from Yildiz Technical University, Istanbul, Turkey, in 2001, and the M.S. and Ph.D. degrees in electrical engineering from Syracuse University, Syracuse, NY, USA, in 2005 and 2008, respectively. From 2008 to 2013, he was with Skyworks Solutions Inc., Cedar Rapids, IA, USA, as a Senior RFIC Design Engineer. From 2013 to 2020, he was a Principal Design Engineer with Hittite Microwave Corporation, Chelmsford, MA, USA; and Analog Devices Inc., Istanbul, Turkey. Over the years, he designed and released many RFIC and MMIC products on CMOS, SiGe, SOI, GaN, and GaAs technologies. In 2020, he joined the Department of Electrical and Electronics Engineering, Istanbul Medipol University, Istanbul, as an Assistant Professor. He has established the RFMicroSense Research Group, where he conducts research on the design and modeling of RF and microwave integrated circuits, devices, systems, and antennas. His dissertation on Low Power CMOS Receiver for Medical Implant Devices was the recipient of the Best Thesis Award. He is currently serving as an Associate Editor for the *Applied Computational Electromagnetics Society*.

HASSAN SANI ABUBAKAR received the bachelor's degree from the Department of Electrical Engineering, Kano State University of Science and Technology (KUST), Wudil, in 2016, and the master's degree in information and communication engineering from the University of Electronics Science and Technology of China (UESTC), in 2020, where he is currently pursuing the Ph.D. degree with the School of Electronics Science and Engineering. His research interests include MIMO antenna designs and 5G antennas.

NASER OJAROUDI PARCHIN (Senior Member, IEEE) received the Ph.D. degree in electrical engineering from the University of Bradford, U.K. He is currently an Assistant Professor (a Lecturer) with Edinburgh Napier University, U.K. He was a Post-Doctoral Research Assistant with the Faculty of Engineering and Informatics, University of Bradford. He was a Research Fellow in the SATNNEX V Project, funded by the European Space Agency. From 2018 to 2020, he was a Marie Curie Research Fellow in the H2020-ITN-SECRET Project, funded by EU Commission, targeting 5G mobile small cells. From 2014 to 2018, he was with the APMS Section, Aalborg University, Denmark. In 2016, he was a Visiting Researcher with Ankara University, Turkey. He has over 12 years of research experience in antennas and microwave engineering. He is the author or coauthor of several books/book chapters and more than 300 technical journals and conference papers. His research interests include phased arrays, MIMO systems, smartphone antennas, SAR/user-impact, full-duplex diversity, 5G antennas, implementable and biomedical sensors, RFID tag antennas, millimeter-wave and terahertz components, fractal structures, metamaterials/metasurfaces, PCB realization, fabry resonators, EBG/FSS-inspired radiators, microwave filters, reconfigurable structures, and wireless propagation. He is a member of the Marie Curie Alumni Association (MCAA) and the European Association on Antennas and Propagation (EurAAP). He was a recipient and a co-recipient of various awards and grants for research publications, such as the 2018 Research Development Fund; the 2020/2021 MDPI Travel Award; and the Best Paper Awards at URSI Symposium 2019, 5G Summit 2019, U.K. URSI Festival 2020, IMDC 2021, and ITC-Egypt 2022. He was included in the Worlds Top Scientists list in 2016, 2020, 2021, and 2022. His papers have more than 6300 citations with H-index is 45, reported by Google Scholar. His score is higher than 95. He is a Research Grant Reviewer of the Dutch Science Council (NWO). He is also an active reviewer in various high-ranking journals and publishers, such as IEEE TRANSACTIONS, IEEE ACCESS/Letters, IET, Wiley, Springer, Elsevier, and MDPI. He is appointed as a guest editor and topic board of several MDPI journals.

HATEM RIMLI (Senior Member, IEEE) received the B.S. degree in physics from the Science Faculty of Monastir, Tunisia, in 1995, the D.E.A. Diploma (master's) degree in quantum mechanics from the Science Faculty of Tunis, Tunisia, in 1999, and the Ph.D. degree in physics (electronics) from the University of Bordeaux 1, France, in 2004. From December 2004 to March 2005, he was a Research Assistant with the PIOM Laboratory, University of Bordeaux 1. From March 2005 to March 2007, he was a Postdoctoral Fellow with the Rennes Institute of Electronics and Telecommunications, France. From March to September 2007, he was a Postdoctoral Fellow with the ESEO Engineering School, Angers, France. From September 2007 to August 2012, he was an Assistant Professor with the Department of Electronics and Telecommunications, Mahdia Institute of Applied Science and Technology (ISSAT), Tunisia. Currently, he is a Professor with the Electrical and Computer Engineering Department, Faculty of Engineering, King Abdulaziz University, Jeddah, Saudi Arabia. His research interests include applied electromagnetic applications, including antennas, metamaterials, and metasurfaces. The main targeted applications are reconfigurable antennas for multi-standard wireless communications systems, security of chipless RFID systems with fractal tags, terahertz photoconductive antennas for infra-red energy harvesting, UWB nano rectennas for collection of solar energy, phase shifters for low-cost 5G communication systems, and microwave absorbing materials for stealth technologies.

BANDAR HAKIM received the Ph.D. degree in electro physics from the University of Maryland. He was with the Medical Robotics Group, École Polytechnique Fédérale de Lausanne, Switzerland; the Center for Devices and Radiological Health, Food and Drug Administration, Washington, DC, USA; and the Neurology Department, Mount Sinai School of Medicine, New York, NY, USA. He served as an industrial consultant in the U.S., Switzerland, and Germany. He is an Assistant Professor of electro physics with King Abdulaziz University.